

1
2
3
4
5
6
7
8
9
10
11
12
13
14
15
16
17
18
19
20
21
22
23

Global Biogeochemical Cycles

Supporting Information for

**Impact of Lagrangian Sea Surface Temperature Variability on Southern Ocean
Phytoplankton Community Growth Rates**

Jessica Zaiss¹, Philip W. Boyd², Scott C. Doney³, Jon N. Havenhand⁴, Naomi M. Levine⁵

¹Department of Earth Science, University of Southern California

²Institute for Marine and Antarctic Studies, University of Tasmania

³Department of Environmental Sciences, University of Virginia

⁴Department of Marine Science, University of Gothenburg

⁵Department of Marine and Environmental Biology, University of Southern California

Contents of this file

Text S1 to S7

Table S1

Figures S1 to S23

24 **Introduction**

25 This supplemental material contains the results of the sensitivity analyses we performed on
26 thermal niche width, final SST in the idealized simulations, and the magnitude of the imposed
27 minimum biomass, as well as the statistical analysis to determine the significance, or lack of, the
28 differences between the sensitivity tests and the results in the main text. Also included are figures
29 to supplement the findings in the main text such as results for the broad shaped reaction norms
30 and the decrease Δ SST results for the skewed reaction norms.

31

32 **S.1 Impact of final temperature in the idealized simulations**

33 To assess the sensitivity of our choice of final SST of 15°C for the idealized simulations, we
34 performed 100 idealized simulations with final SSTs of 10°C and 20°C with the same rates and
35 magnitudes of temperature change as presented in the main text. Specifically, we compared the
36 percent difference between the individual-based model and the Q_{10} parameterization, relative to
37 Q_{10} , at the timestep when SST stabilizes as well as the length of time it took for the community
38 growth rates to equilibrate to steady conditions, referred to as the memory length in the main
39 text.

40 The final SST of the idealized profiles did not impact the results of our study. The offset between
41 the Q_{10} parameterization and the individual-based model remained statistically similar (95% CI,
42 see section S.7 for description of statistical analyses) for all the simulations (Figure S1).
43 Additionally, because the results are presented in terms of generations rather than absolute time,
44 the length of the memory effect is also statistically the same (95% CI) for all simulations (Figure
45 S2).

46

47 **S.2 Impact of thermal niche width in idealized simulations**

48 The width of the thermal niche had a varying, but predictable, impact on the percent difference
49 from Q_{10} . To test the impact of the thermal niche width, we ran 100 simulations of the same
50 idealized SST profiles as in the main text with both narrower and wider thermal niches for the
51 individuals. Making the thermal niche more narrow (10.5°C) relative to the simulations in the
52 main text (thermal niche = 14°C) did not have a significant (95% CI) impact on the percent
53 difference between the individual-based model and the Q_{10} growth parameterization, for either
54 shape of reaction norm (Figure S3, left column). Increasing the thermal niche from 14°C to
55 20.5°C (Figure S3, right column) also did not have a significant impact on the offset from the Q_{10}
56 parameterization for skewed reaction norms (95% CI) but did for the broad reaction norms (95%
57 CI). A wider thermal niche for the broad reaction norms decreased the percent difference from
58 Q_{10} by an average of 10.1% with simulations in which ΔSST changed over 7 days experiencing
59 the largest decreases of up to 29.4%.

60

61 The width of the thermal niche in conjunction with the magnitude of SST change impacted the
62 memory length. For small ($2\text{-}3^{\circ}\text{C}$) and large ($8\text{-}9^{\circ}\text{C}$) SST changes, wider thermal niches
63 produced shorter memory effects (95% CI) by an average of $2.1 \text{ generations} \pm 3.4 \text{ generations}$
64 (1σ) for the broad reaction norms and $0.6 \text{ generations} \pm 1.6 \text{ generations}$ (1σ) for the skewed
65 reaction norms. Conversely, wider thermal niches that experienced moderate SST changes (4-
66 7°C) had longer memory effects than the default thermal niches by $1.8 \text{ generations} \pm 4.0$
67 generations (1σ) for the broad and $0.5 \text{ generations} \pm 1.0 \text{ generations}$ (1σ) for the skewed reaction
68 norms. This was seen across both sets of simulations for the broad reaction norms (Figure S4,
69 bottom row). For skewed reaction norms, decreasing the thermal niche width relative to the
70 default width did not have a significant impact on the memory length (95% CI) (Figure S4, top
71 row). Regardless of thermal niche width, the overall relationship between memory length and the
72 rate and magnitude of SST change was the same as the simulations in the main text and did not
73 change our results or conclusions.

74

75 For broad shaped reaction norms, wider thermal niches mean that individuals were able to
76 continue to grow over a larger span of SSTs on either side of their optimum growth temperature
77 (T_{opt}) compared to individuals with narrower thermal niches. When temperature changes were
78 small ($2\text{-}3^{\circ}\text{C}$), the biomass weighted community growth rate was able to better track small
79 changes in SST because the SST did not go outside of the thermal niche. Similarly, for large SST
80 changes ($8\text{-}9^{\circ}\text{C}$), the community was able to respond to the SST changes more quickly than a
81 community with a narrower thermal niche because more individuals were able to grow at the
82 final SST. When SST changes were more moderate ($4\text{-}6^{\circ}\text{C}$), the individuals in the original
83 environment could continue to grow over a larger range of temperatures past their T_{opt} which
84 meant that those best suited for the new environment had more biomass to overcome before
85 making a significant contribution to the biomass-weighted community growth rates compared to
86 individuals in a community with narrow thermal niches.

87 The memory length for the skewed reaction norms was less affected by the width of the thermal
88 niche due to the asymmetry of the reaction norm shape. By increasing the width the reaction
89 norm, but keeping the maximum growth rate and T_{opt} the same, the part of the reaction norm that
90 was extended corresponded to relatively low growth rates. So even though individuals could
91 grow at a larger temperature range, that growth did not have a large impact on the memory
92 length.

93

94 The impact of thermal niche width on the difference from Q_{10} and the length of the memory
95 effect did not change any of the conclusions of the manuscript. Across all the simulations, larger
96 and faster SST changes resulted in the largest offsets from Q_{10} and moderate SST changes
97 induced the longest memory effects.

98

99 S.3 Model sensitivity to minimum biomass parameter

100 In the main text, we imposed a minimum biomass of $0.001 \text{ mmol C m}^{-3}$ such that no individual
101 was allowed to go extinct, akin to the “everything is everywhere” principle (Hutchinson, 1961).
102 To test the sensitivity of our results to this parameter, we ran 100 simulations with the same
103 idealized SST profiles with a minimum biomass of $0.0001 \text{ mmol C m}^{-3}$, an order of magnitude
104 smaller. For both the skewed shaped and broad shaped reaction norms, lower minimum biomass
105 generally increased both the offset from Q_{10} simulated growth rates (95% CI, Figure S5) and the
106 memory length (95% CI, Figure S6). The difference from Q_{10} increased by an average of 1.5%
107 $\pm 8.6\%$ (1σ) for the broad and $2.6\% \pm 8.9\%$ (1σ) for skewed shaped reaction norms, but ranged as
108 high as 31.7% (broad) and 27.3% (skewed). For small ΔSSTs ($2\text{-}3^\circ\text{C}$), lower minimum biomass
109 slightly decreased the difference between Q_{10} simulated growth but as ΔSSTs increased, so did
110 the offset. Memory lengths increased by an average of 4.0 ± 4.1 (1σ) generations for the broad
111 reaction norms and 3.0 ± 3 (1σ) generations for the skewed reaction norms, but ranged as high as
112 12.6 generations (broad) and 10.6 generations (skewed) longer for the smaller minimum
113 biomass. A lower minimum biomass meant that individuals with the minimum biomass
114 contributed less to the overall biomass-weighted community growth rate, resulting in lower
115 growth rates and larger departures from Q_{10} . This also meant that those individuals best suited
116 for the new environment started growing with lower biomass and thus took longer to overcome
117 the previously accumulated biomass from the initial conditions which resulted in longer memory
118 lengths. As such, the results presented in the main text are a conservative estimate of the
119 difference from Q_{10} and memory length.

120 The overall patterns remained the same between both minimum biomass simulations. The
121 direction of the ΔSST change did not impact the memory length for the broad reaction norms
122 whereas decreasing ΔSSTs yielded longer memory lengths for the skewed reaction norms for
123 both sets of simulations. In both sets of simulations, the moderate ΔSSTs resulted in the longest
124 memory lengths.

125

126 **S.4 Comparison of Ecosystem Model Choice**

127 We compared the community growth rates from several different models to ensure that the
128 results we found were not the result of our choice of model. We found that all models showed
129 similar responses in community growth rate. Below is a description of each of the models used in
130 this comparison.

131

132 The biomass of each individual (P_i , in mmol C m^{-3}) was calculated as

133

$$134 \quad \frac{dP_i}{dt} = \mu_i * P_i - loss \quad \text{Eq. S1}$$

135

136 where $\mu_{i,t}$ (day^{-1}) is the individual growth rate at time t . Here we investigated different
137 formulations for the loss term.

138

139 **Linear Mortality**

140 We started with simple linear mortality, where loss scales linearly with biomass, similar to
141 Moisan et al. (2002).

142

$$143 \quad \frac{dP_i}{dt} = \mu_i * P_i - m * P_i \quad \text{Eq. S2}$$

144

145 We found that, the mortality had to be set to unrealistic values (approx. equal to Q_{10} values) in
146 order to keep biomass from exponentially increasing. However, this model does still show a dip
147 in community growth rates with changes in SST that is described in the main text.

148

149 **Quadratic Mortality (used in the main text)**

150 A more common approach is to represent loss as a quadratic mortality:

$$151 \quad \frac{dP_i}{dt} = \mu_i * P_i - m * P_i^2 \quad \text{Eq. S3}$$

152 Simulating phytoplankton loss as quadratic mortality showed the same dip in community growth
153 rates as SSTs begin to as described in the main text. The overall magnitude of the loss term is
154 consistent with the other models also.

155

156 **Simple Ecosystem**

157 We also tested a more complex ecosystem model with linear mortality and loss due to grazing.

158

$$159 \quad \frac{dP_i}{dt} = (\mu_i - m) * P_i - g * \frac{P_i}{P} * Z * P_i \quad \text{Eq. S4}$$

160

161 where g is the temperature dependent grazing ($\text{m}^3 \text{mmol C}^{-1} \text{day}^{-1}$) and Z is the total zooplankton
162 biomass (mmol C m^{-3}). To keep our phytoplankton and zooplankton growth internally
163 consistent, we simultaneously solve for the change in total phytoplankton biomass (P) and
164 zooplankton biomass (Z) over time (where $P = \sum P_i$ for individuals whose biomass is greater
165 than the minimum) using the following equations:

$$166 \quad \frac{dP}{dt} = \lambda * P - g * Z * P \quad \text{Eq. S5}$$

$$167 \quad \frac{dZ}{dt} = 0.3 * g * Z * P - m_z * Z \quad \text{Eq. S6}$$

168

169 where λ (day^{-1}) is the biomass weighted community growth rate from all $P_i >$ minimum biomass,
170 0.3 is the zooplankton efficiency, and m_z is the zooplankton mortality rate (day^{-1}). Re-solving for
171 total P instead of using the sum of the individual biomasses allowed us to avoid issues with
172 resetting low biomass individuals to the minimum biomass which constantly adds biomass to the
173 system. This resulted in predator-prey oscillations (Figure S7) but also showed the dip in
174 community growth rates as SSTs began to change.

175

176 **Constant grazing**

177 This model followed the same equations outlined for the Simple Ecosystem model above, but
178 instead of solving for how zooplankton biomass changes over time, we calculate Z for each
179 timestep as:

$$180 \quad Z = -0.0187 * \lambda + 5 * \frac{\lambda}{a} \quad \text{Eq. S7}$$

181 where λ (day^{-1}) is the community growth rate defined in the main text (Equation 5) and a (day^{-1})
182 is the growth rate from the Q_{10} parameter (Equation 2). This formulation provided a relatively
183 constant grazing pressure which prevented predator-prey oscillations. As seen with the other
184 formulations, this resulted in a decrease in community growth rates as SSTs change.

185

186 **S.5 Statistics Calculations for Sensitivity Tests**

187 To calculate the potential significance of results from the sensitivity tests, we performed Type II
188 linear regression and tested the significance of the slope against a value of 1. The regression was
189 performed using the *lsqfitma* function in Matlab made available from the Monterey Bay
190 Aquarium Research Institute (<https://www.mbari.org/index-of-downloadable-files/>). This
191 provided a slope and the uncertainty on that slope. Using these data, we then calculated the Z test
192 statistic as:

193
$$Z = \frac{x - \mu}{\sigma \sqrt{\frac{1}{N}}} \quad \text{Eq. S8}$$

194

195 where x is the slope to test against, here set to one, μ is the slope from the Type II regression, σ is
196 the standard deviation on the slope, and N is the number of independent tests to find μ , which is
197 one for the *lsqfitma* regression. Once Z is calculated, we compare this to the standard score based on a
198 95% confidence interval which corresponds to a standard score of ± 1.96 . If Z is outside of this range, we
199 reject the null hypothesis that the slope, μ is equal to one. Otherwise, we fail to reject the null
200 hypothesis.

201

202 **S.7 Acclimation Rates**

203 To test the impact of different acclimation timescales we performed sensitivity tests in which we
204 imposed systematic acclimation rates for all phenotypes in the model ranging from $0.2\text{ }^{\circ}\text{C day}^{-1}$
205 to $0.6\text{ }^{\circ}\text{C day}^{-1}$ in increments of $0.1\text{ }^{\circ}\text{C day}^{-1}$. These rates are consistent with acclimation rates
206 determined for the Southern Ocean diatom *F. cylindrus* (Robert Strzepek, personal
207 communication). We then ran the model with the idealized SST profiles for a $\Delta\text{SST} = 2^{\circ}\text{C}$ in 7
208 days ($0.29\text{ }^{\circ}\text{C day}^{-1}$), 3°C in 7 days ($0.43\text{ }^{\circ}\text{C day}^{-1}$), 4°C in 7 days ($0.57\text{ }^{\circ}\text{C day}^{-1}$) and 5°C in 21
209 days ($0.24\text{ }^{\circ}\text{C day}^{-1}$). These intervals corresponded to the magnitudes and rates of change most
210 commonly experienced by the drifter trajectories (see Section 3.1) for which the rate of change
211 was greater than $0.2\text{ }^{\circ}\text{C day}^{-1}$.

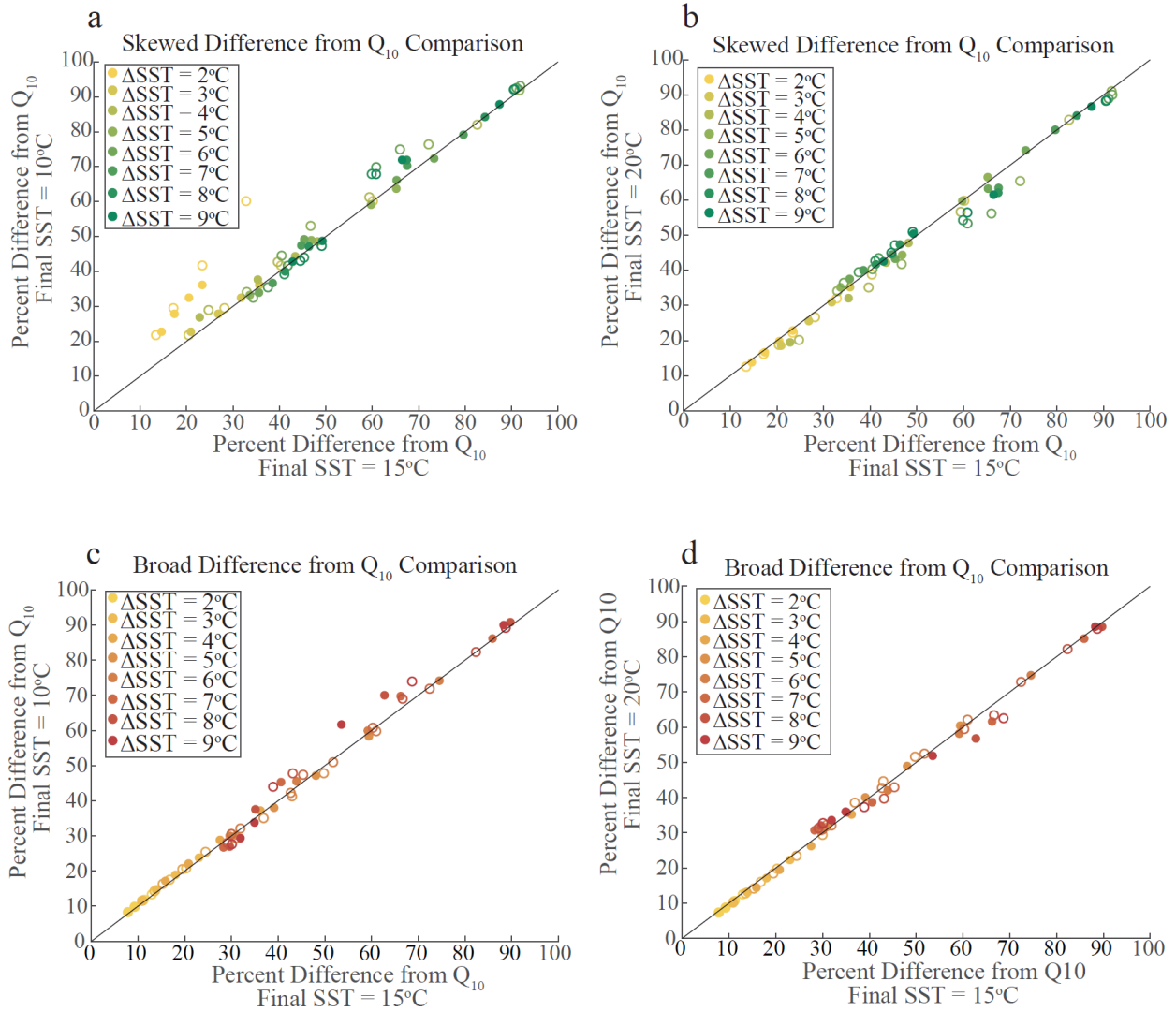
212

213 Acclimation in the model was represented as a linear rate of change with the growth rate
214 following the thermal reaction curve. Specifically, if SST rapidly changed from 15°C to 16°C in
215 one day, a phenotype with an acclimation timescale of $0.2^{\circ}\text{C day}^{-1}$ would move from the growth
216 rate at 15°C to the growth rate at 15.2°C . If the SST then held constant at 16°C , the phenotype
217 would acclimate by the end of the fifth day.

218

219 Table S1. Table S1. Results of SST_{max} variability analysis.

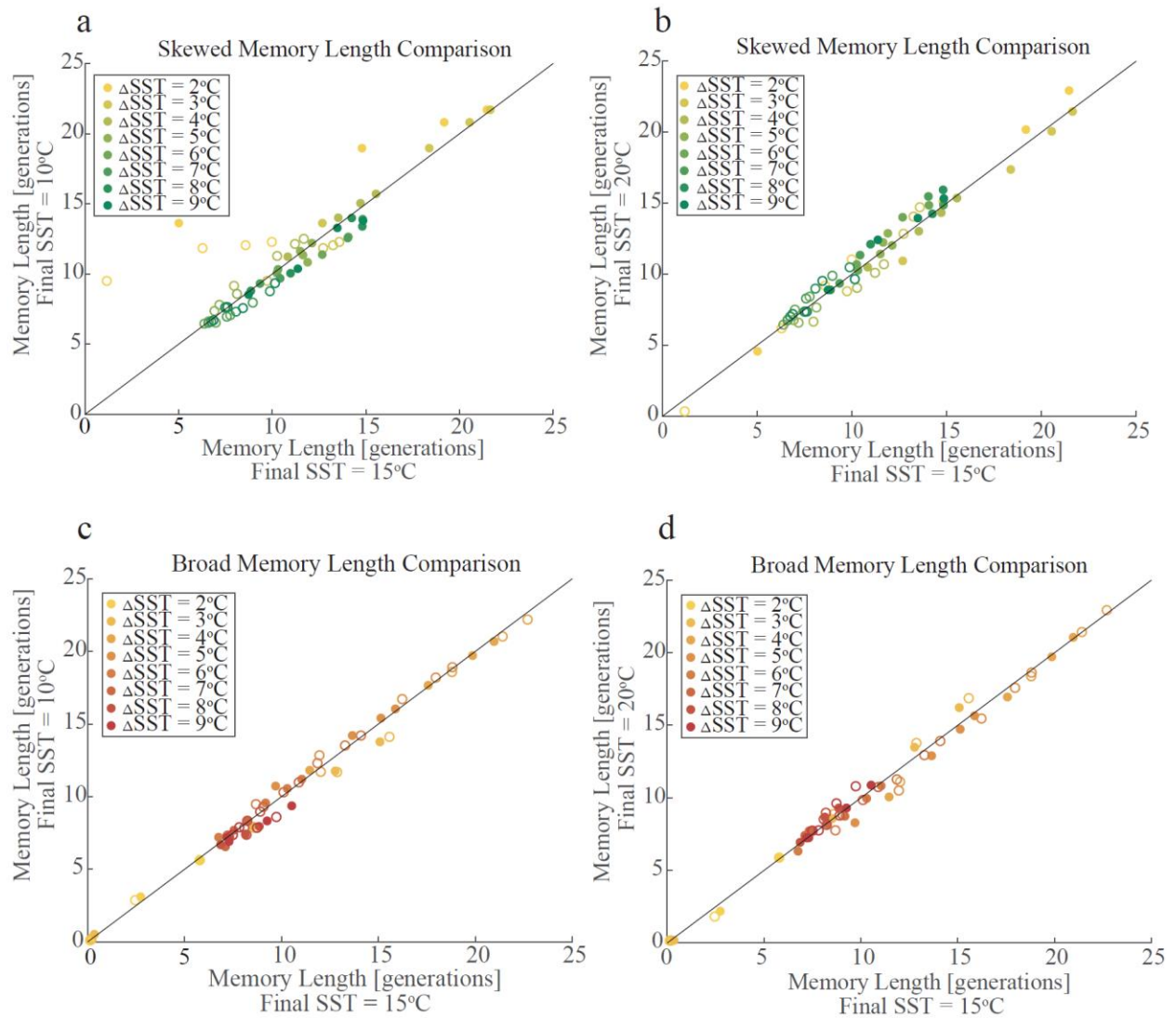
	7 days	21 days	45 days	90 days
# of data points	729,262	465,785	273,997	1593
Mean Δ SST _{max} , °C	0.9	1.7	2.7	4.2
Standard Deviation, °C	0.7	1.0	1.5	2.0
Median Δ SST _{max} , °C	0.7	1.5	2.4	3.9
Mode Δ SST _{max} , °C	0.4	1.1	2.0	2.0
Skewness Δ SST _{max}	2.5	1.6	0.9	0.9



221

222 Figure S1. The impact of final SST on percent difference between the individual based model and the Q_{10}
 223 parameterization, relative to Q_{10} . The results from the simulations in the main text are compared to
 224 simulations with final SSTs of 10°C (a,c) and 20°C (b,d) for both the skewed (top row) and broad (bottom
 225 row) shaped reaction norms. Open data points represent decreasing Δ SSTs and filled in data are
 226 increasing Δ SSTs. The black line indicates the 1-1 line. There is no statistical difference between
 227 simulations with differing final SSTs (95% CI).

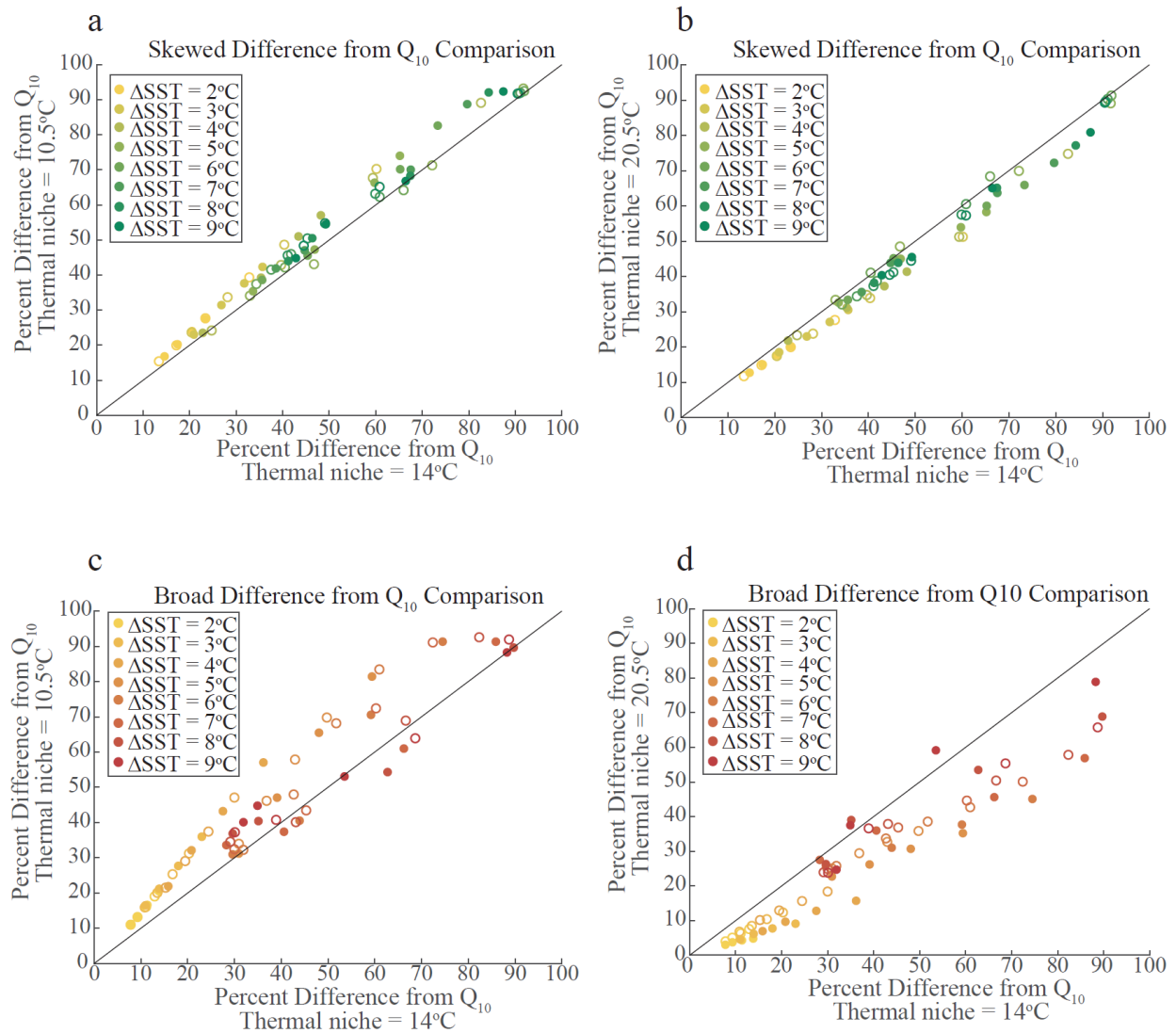
228



229

230 Figure S2. The impact of final SST on memory length. The results from the simulations in the main text
 231 are compared to simulations with final SSTs of 10°C (a,c) and 20°C (b,d) for both the skewed (top row)
 232 and broad (bottom row) shaped reaction norms. Open data points represent decreasing Δ SSTs and filled
 233 in data are increasing Δ SSTs. The black line is the 1-1 line. There is no statistical difference between
 234 simulations with differing final SSTs (95% CI).

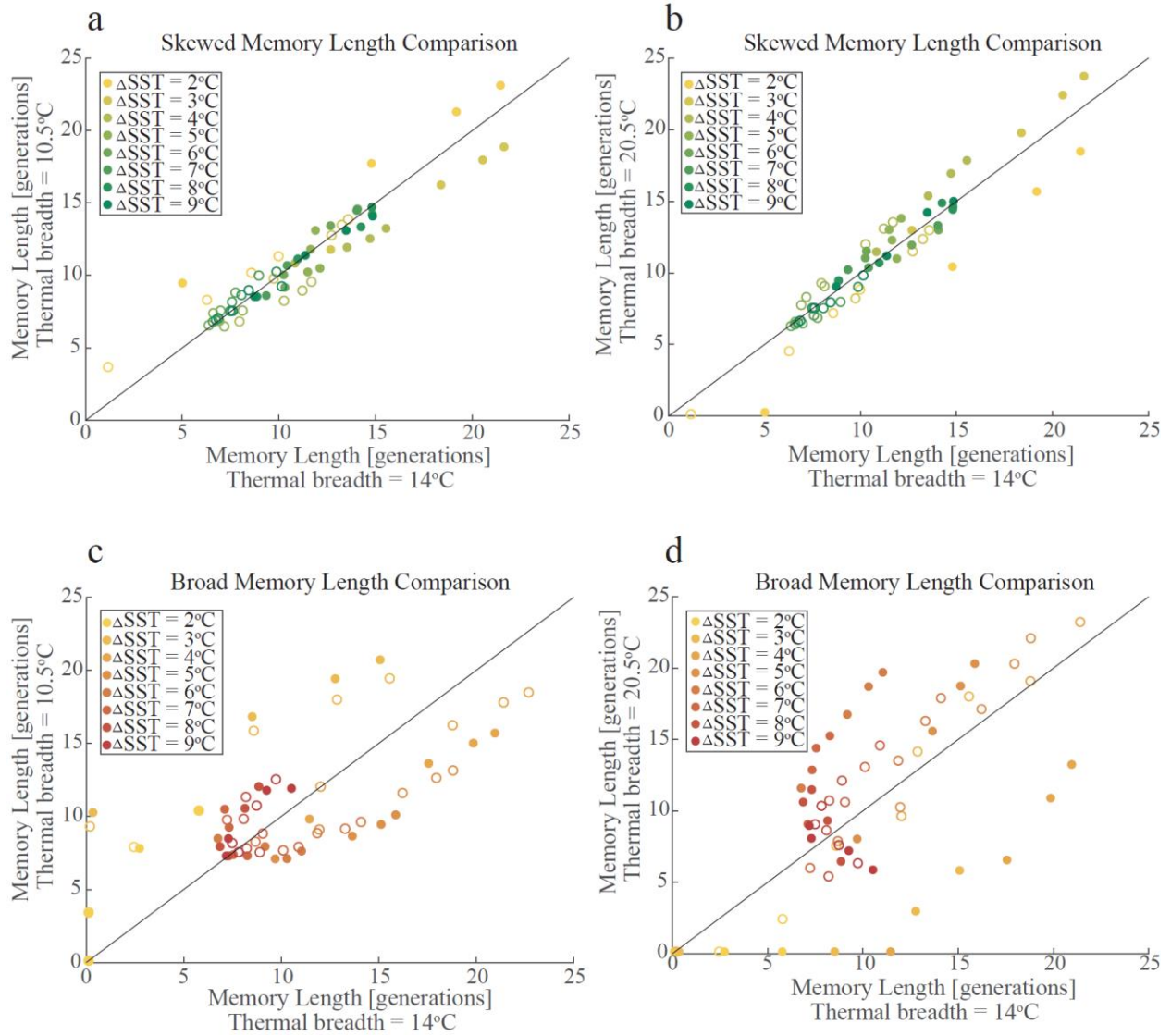
235



236

237 Figure S3. The impact of thermal niche width on percent difference from Q_{10} . The results from the
 238 simulations in the main text are compared to simulations with narrower (a,c) and wider (b,d) for both the
 239 skewed (top row) and broad (bottom row) shaped reaction norms. The black line is the 1-1 line. Closed
 240 data points represent increasing ΔSST s and open circles represent decreasing ΔSST s. For broad reaction
 241 norms, increasing the thermal niche increases the difference from the Q_{10} parameterized growth rates.
 242 There was no significant difference between the simulations for skewed reaction norms.

243

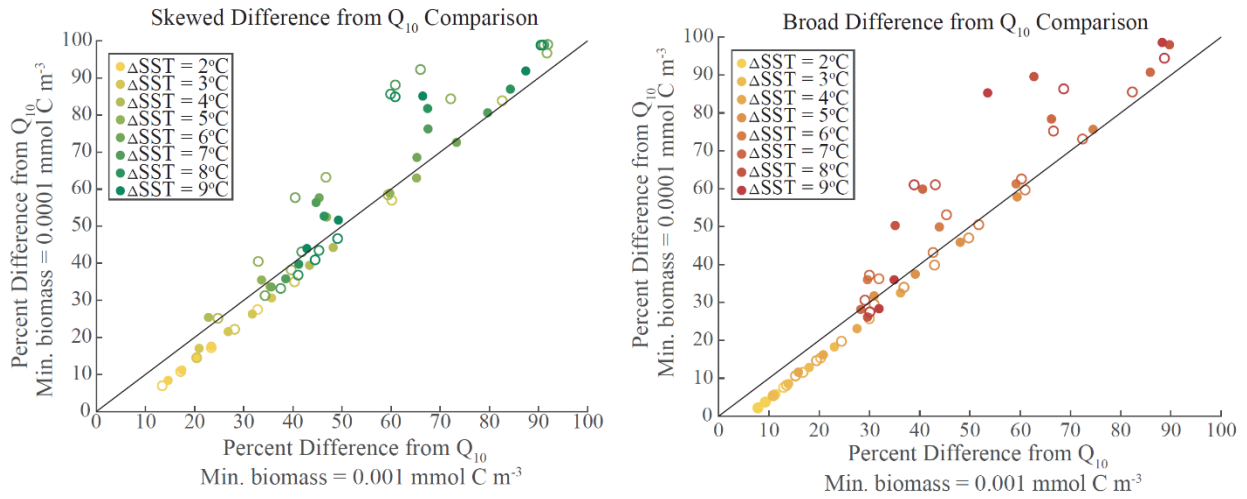


244

245 Figure S4. The impact of thermal niche width on memory length. The results from the simulations in the
 246 main text are compared to simulations with narrower (left column) and wider (right column) for both the
 247 skewed (top row) and broad (bottom row) shaped reaction norms. The black line is the 1-1 line. Closed
 248 data points represent increasing ΔSST s and open circles represent decreasing ΔSST s. Broad reaction

249

250

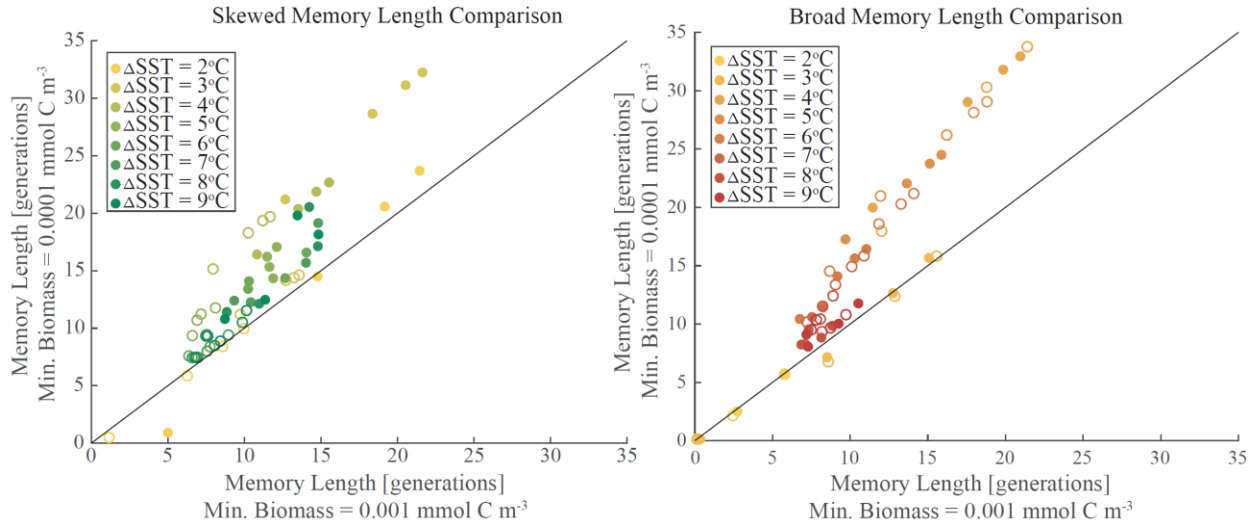


251

252 Figure S5. The impact of minimum biomass on deviation from Q_{10} . The results from the simulations in
 253 the main text (x-axis) are compared to simulations with an order of magnitude smaller minimum biomass
 254 for both skewed (left) and broad (right) shaped reaction norms. The black line is the 1-1 line. Filled in
 255 data points represent increasing ΔSSTs and open data points are decreasing ΔSSTs . The minimum
 256 biomass impact is significant at the 95% CI with an average increase in offset from Q_{10} , for both reaction
 257 norm shapes.

258

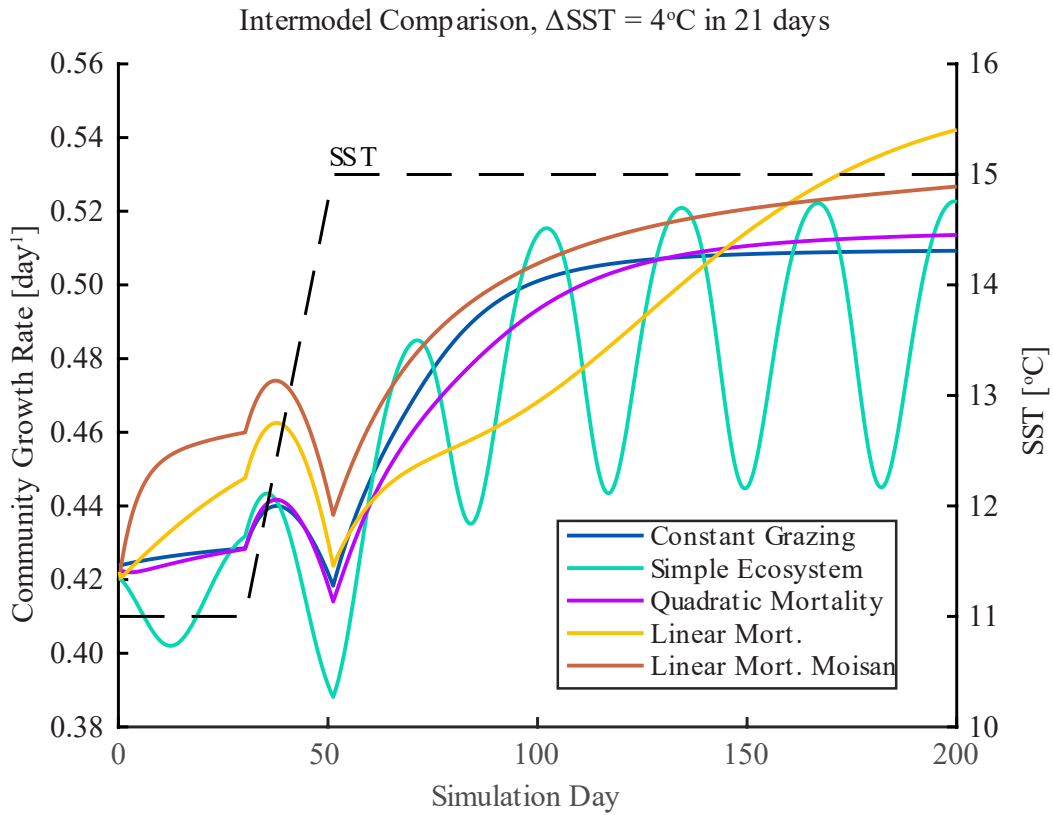
259



260

261 Figure S6. The impact of minimum biomass on memory length. The results from the simulations in the
 262 main text (x-axis) are compared to simulations with an order of magnitude smaller minimum biomass for
 263 both skewed (left) and broad (right) shaped reaction norms. The black line is the 1-1 line. Filled in data
 264 points represent increasing Δ SSTs and open data points are decreasing Δ SSTs. The minimum biomass
 265 impact is significant at the 95% CI with an average increase in memory length for both reaction norm
 266 shapes. However, the pattern of moderate Δ SSTs exhibiting the longest memory effects were robust
 267 across all simulations.

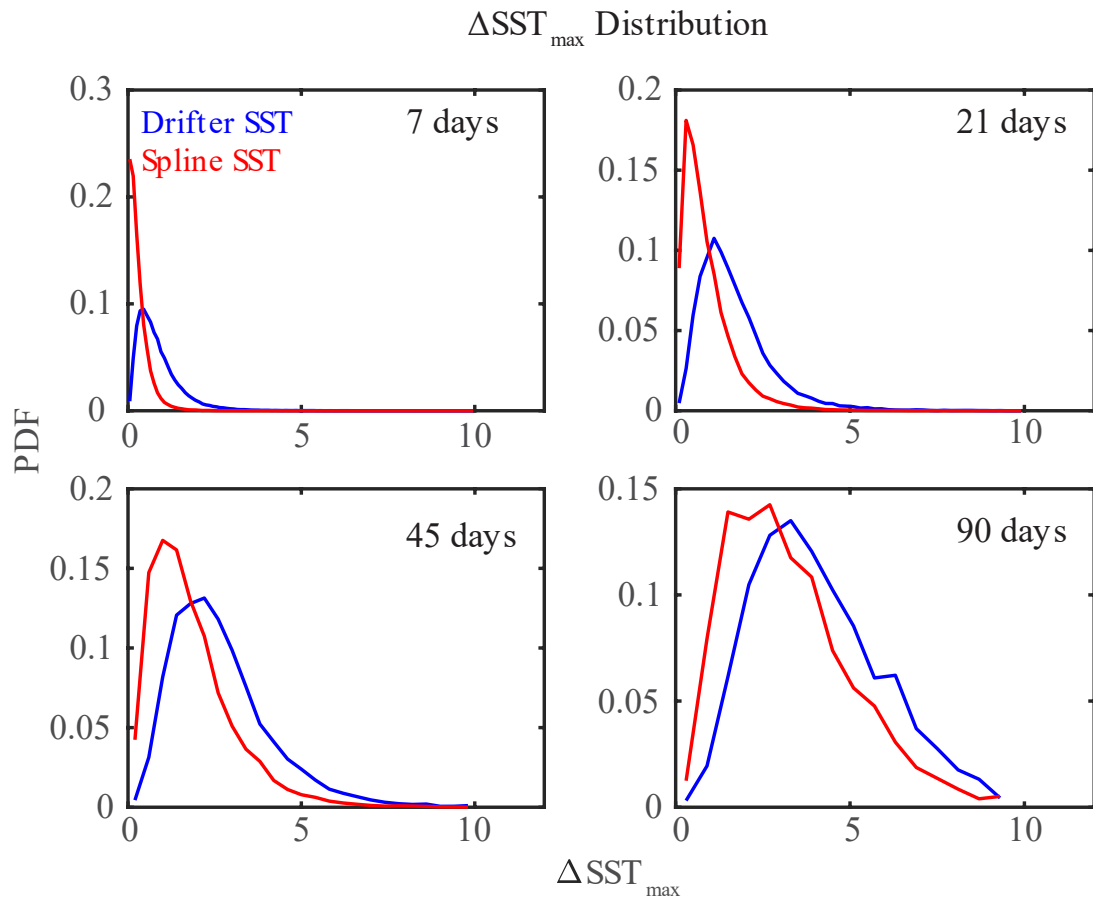
268



269

270 Figure S7. Comparison between different ecosystem model results for community growth for an idealized
 271 simulation with an increase of 4 °C over 21 days. For community growth rates, all models show similar
 272 qualitative results indicating a decrease in growth rate over the transient conditions culminating in a
 273 growth rate minimum when SSTs stabilize.

274

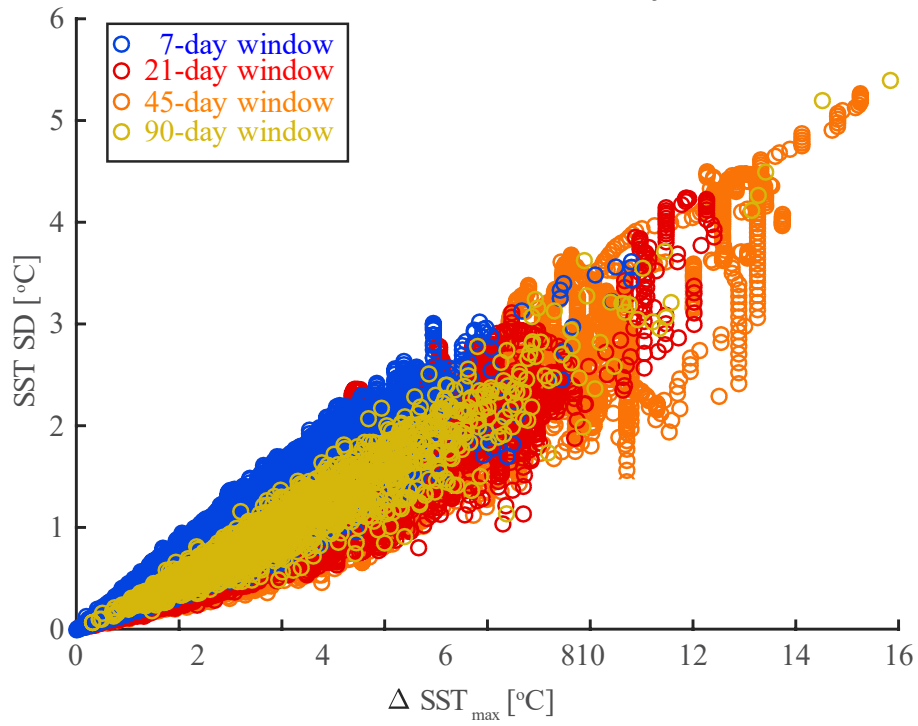


275

276 Figure S8. Probability density functions of the absolute value of the maximum change in SST over 7, 21,
 277 45, and 90 days for the drifter trajectories (blue) and the smoothed splines of the trajectory SSTs (red).

278

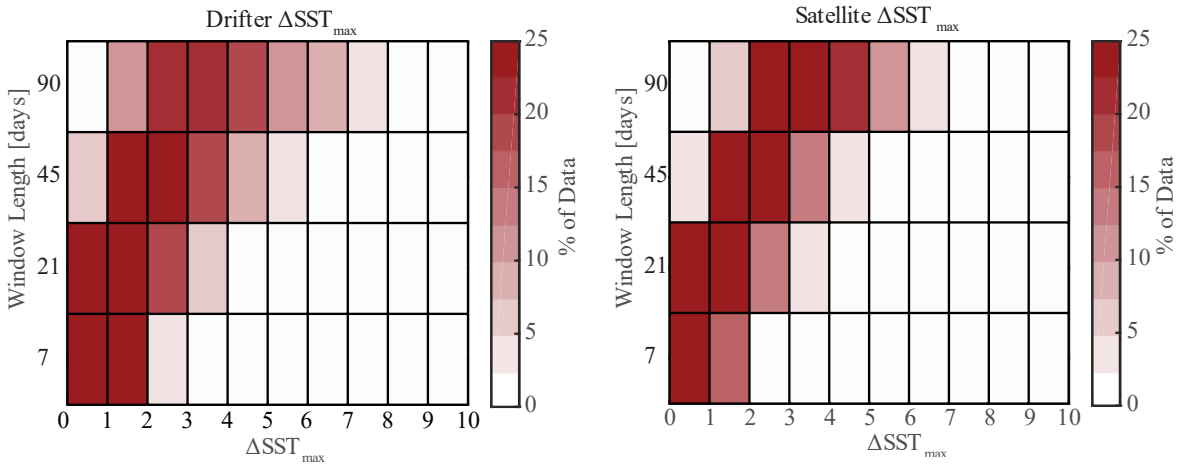
Comparison of $\Delta\text{SST}_{\text{max}}$ and
standard deviation for drifter trajectories



279

280 Figure S9. The standard deviation (1σ) as a function of $\Delta\text{SST}_{\text{max}}$ over different Δt_{max} windows. $\Delta\text{SST}_{\text{max}}$
281 drives the variability across the Δt_{max} window lengths.

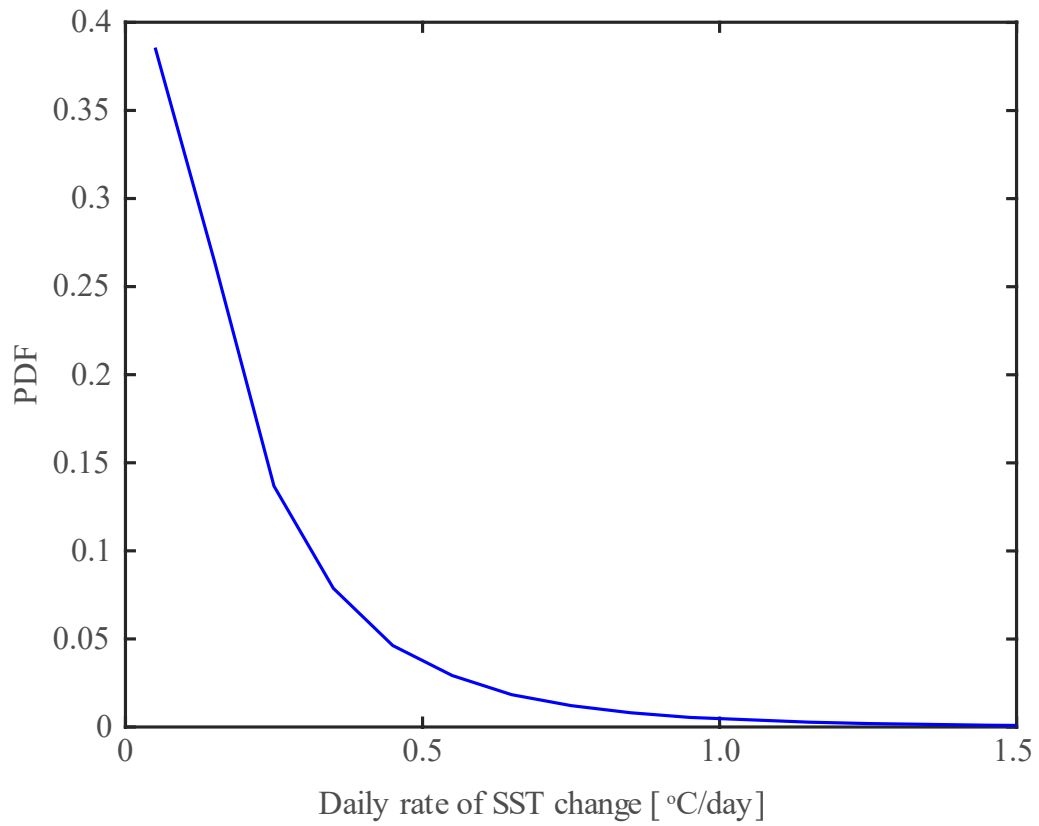
282



283

284 Figure S10. Results from SST variability analyses for the drifter (left) and satellite trajectories (right)
 285 showing most common SST changes for each time window. Data are presented as total percent of data
 286 that fall within that ΔSST bin for the window length. Each row sums to 100%. Although the magnitudes
 287 of variability are similar, the nature of that variability is different with the Lagrangian reference frame
 288 experiencing more variability consistent with longer memory effects.

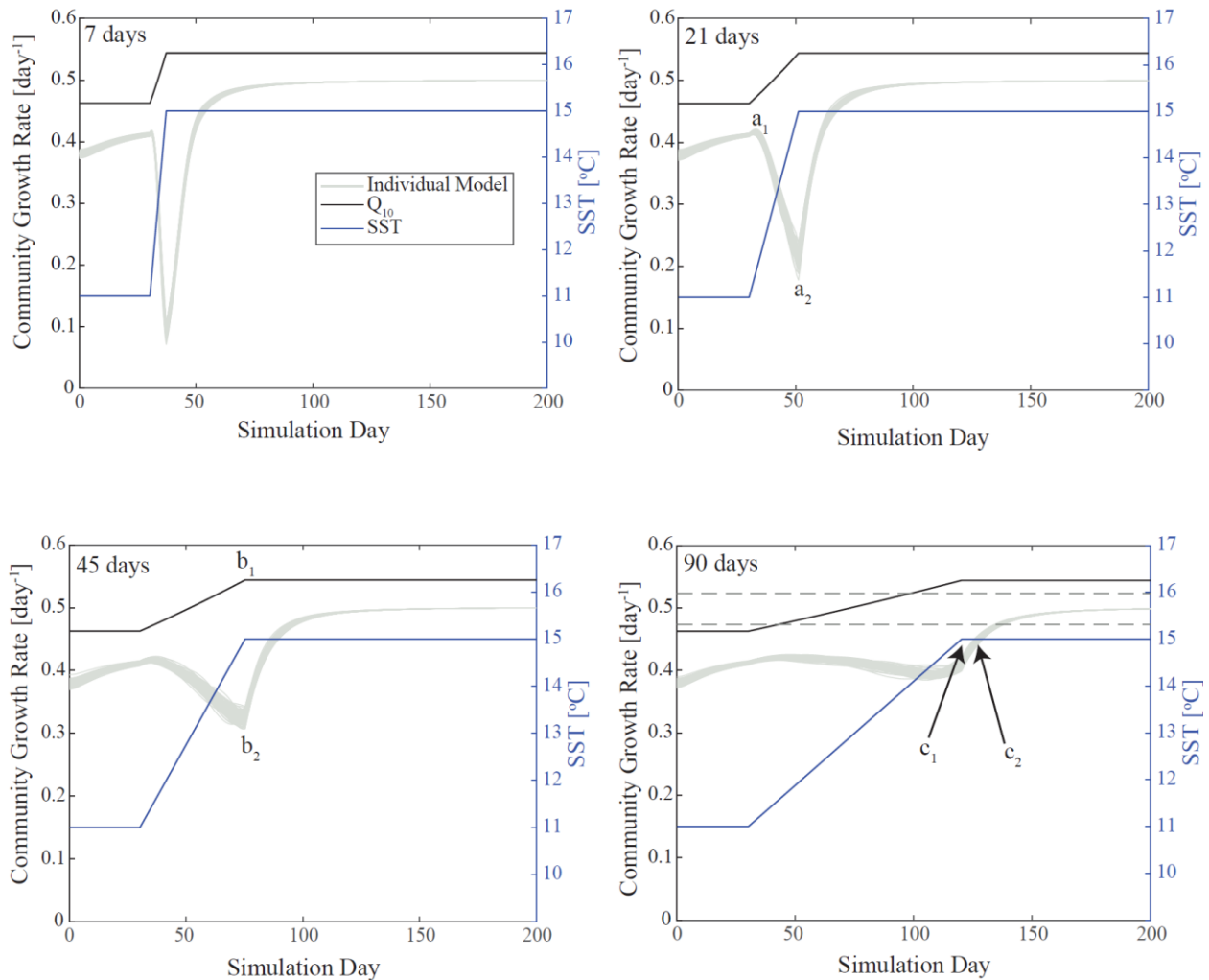
289



290

291 Figure S11. Daily rates of SST change for drifter trajectories. The rates of change were calculated as the
292 range of the recorded SST values over a 1-day moving window for a total of $n = 781,749$ data points for
293 197,100 days.

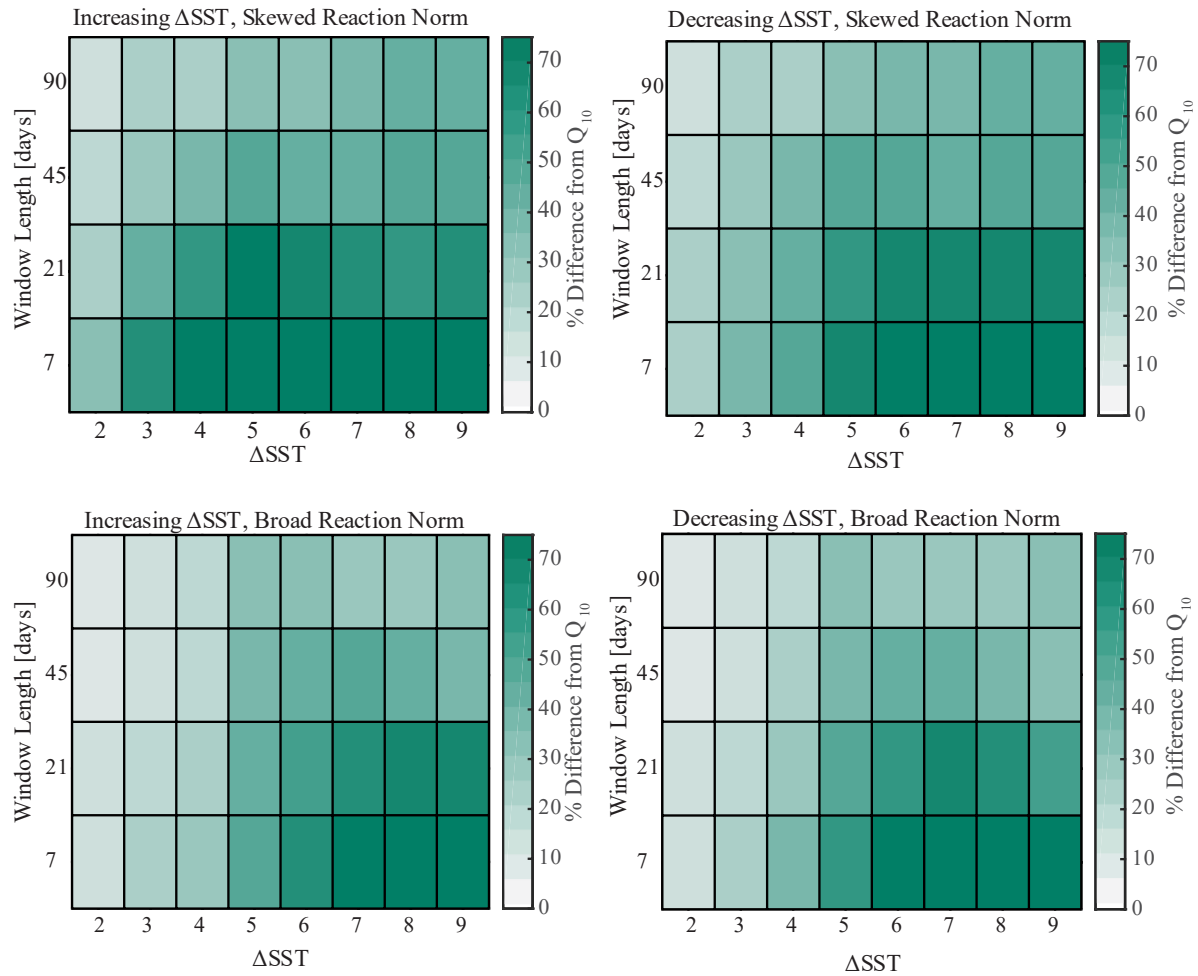
294



295

296 Figure S12. Community growth rates for each of the 100 simulations (grey lines) for an increase of 4°C
 297 over 7, 21, 45, and 90 days for skewed shaped reaction norms. The black line is the Q₁₀ simulated
 298 community growth rate and the blue line is the SST profile for the simulation. The locations marked a₁
 299 and a₂ in the 21-day panel represent the timesteps used to calculate the percent change in growth rate
 300 associated with transient SSTs as shown in Figures 2b. This metric was calculated as $(a_1 - a_2) * 100 / a_1$. The
 301 locations marked b₁ and b₂ in the 45-day panel represent the timesteps used to calculate the percent
 302 difference in growth rates between the Q₁₀ parameterized growth and the phenotype model as shown in
 303 Figure 2c, S11. This metric was calculated as $(b_1 - b_2) * 100 / b_1$. The locations marked c₁ and c₂ in the 90-
 304 day panel point to the timesteps used to calculate the memory length. The dashed grey lines represent
 305 ±5% of the final, stabilized community growth rate which was used as the threshold for the memory
 306 effect which was defined as the time in days between c₁ when SSTs stabilize and c₂ when the community
 307 growth rate crosses the threshold.

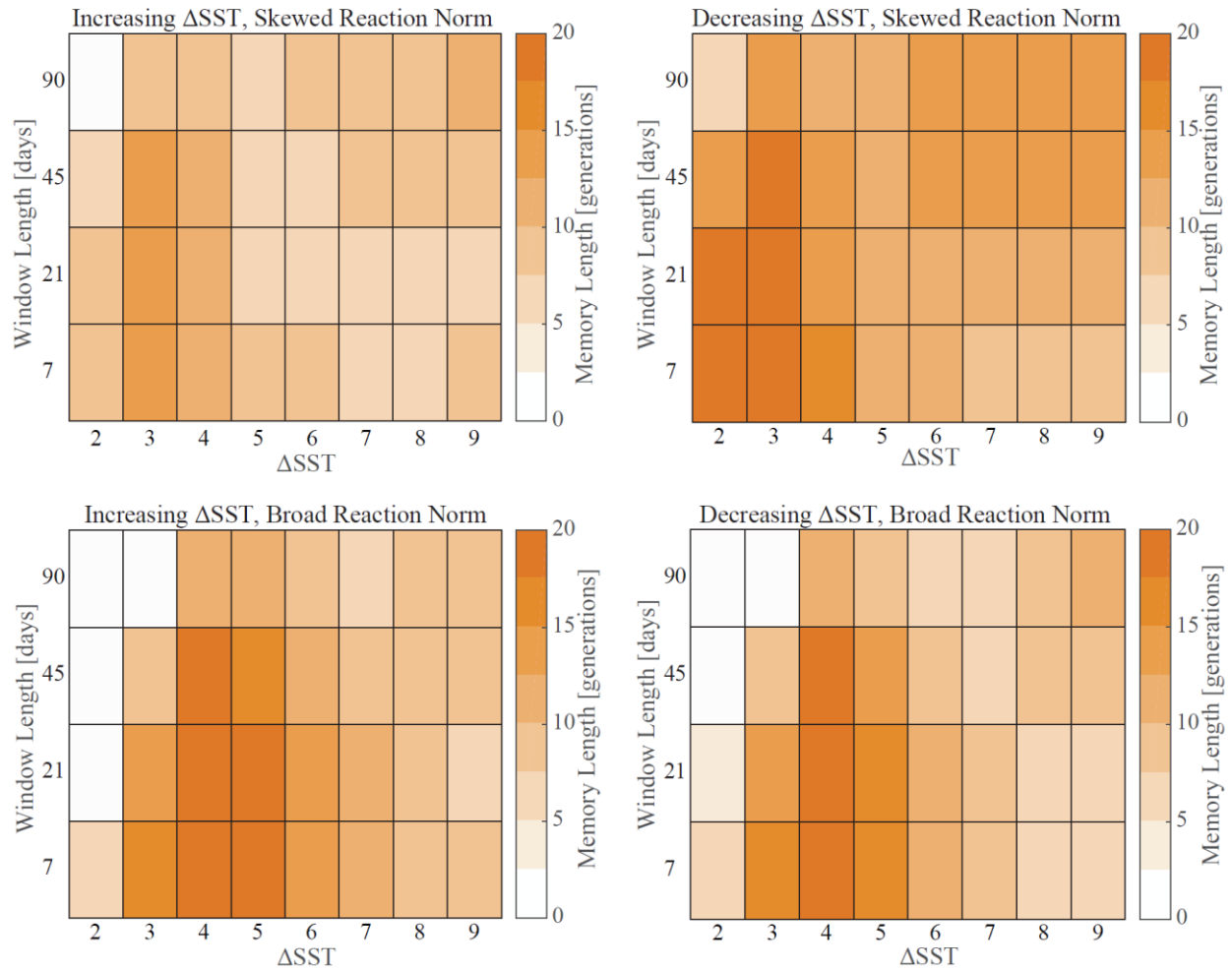
308



309

310 Figure S13. Full results for the percent difference from Q_{10} at the timestep when SSTs stabilize in the
 311 idealized simulations for the skewed shaped reaction norms (top row) and the broad shaped reaction
 312 norms (bottom row) under both increasing SSTs (left column) and decreasing SSTs (right column).

313

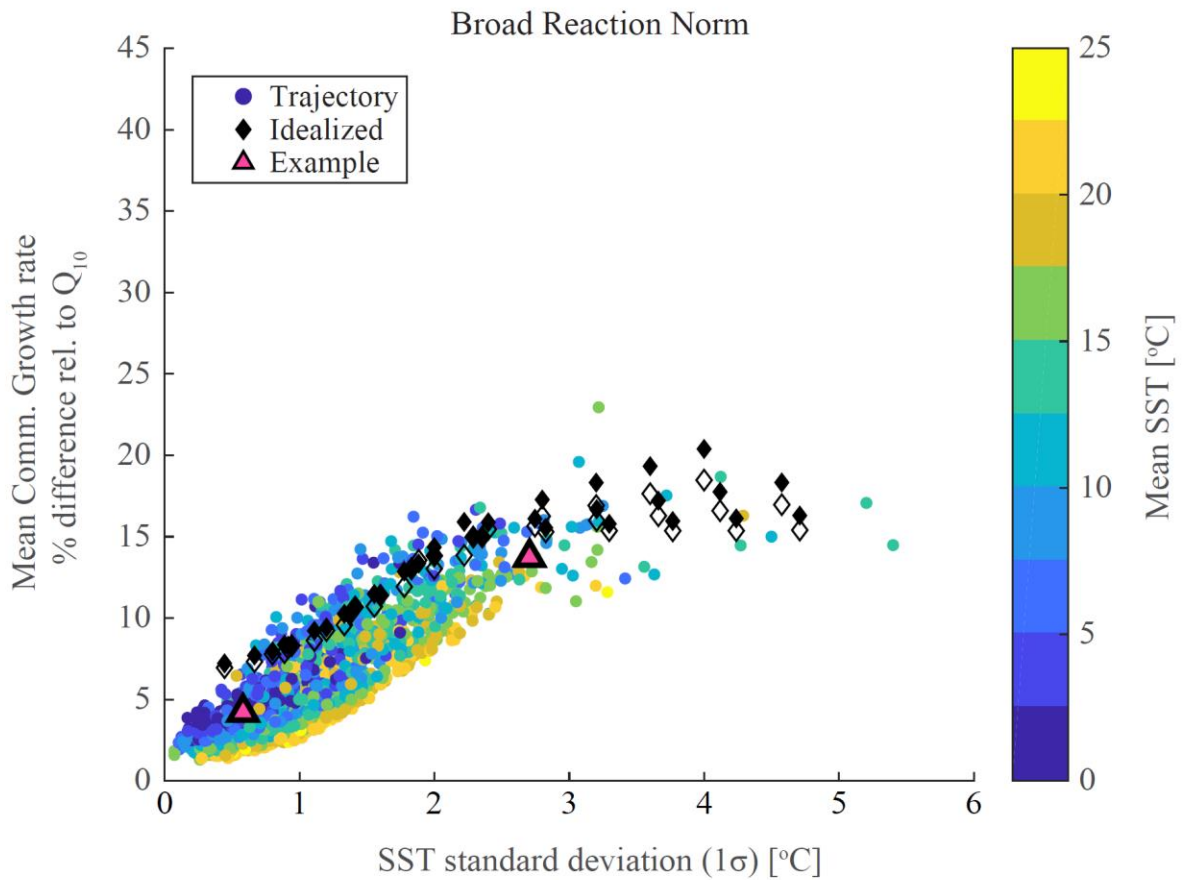


314

315 Figure S14 Full results for the length of the memory effect in the idealized simulations for the skewed
 316 shaped reaction norms (top row) and the broad shaped reaction norms (bottom row) under both increasing
 317 SSTs (left column) and decreasing SSTs (right column).

318

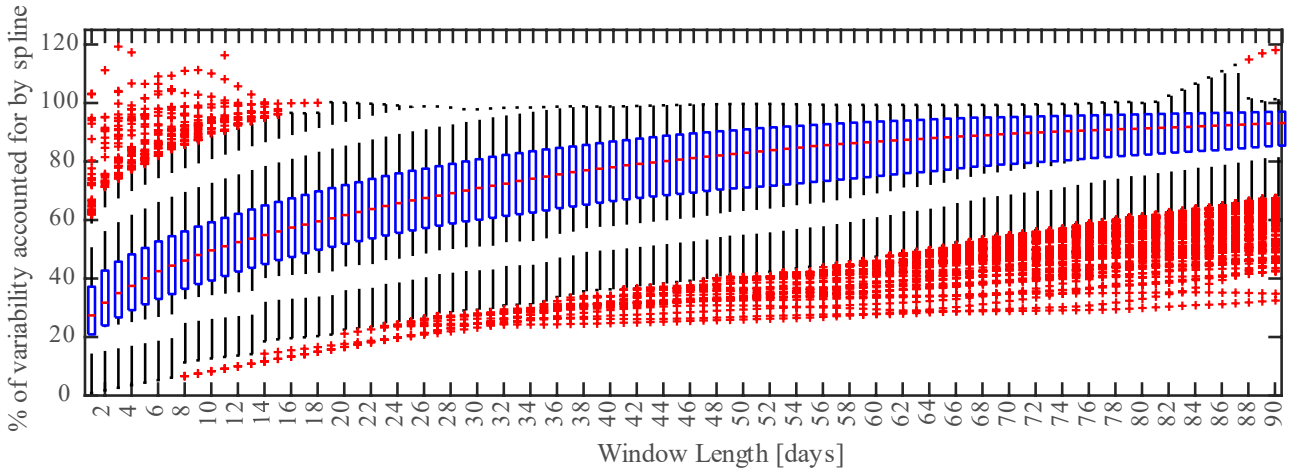
319



320

321 Figure S15. The 90-day average percent difference between community growth rates determined via the
 322 Q_{10} method and the phenotype-based model versus standard deviation (1σ) of SST over the 90-day
 323 trajectory. Drifter data are represented by circles colored according to their mean SST. Black diamonds
 324 represent the first 90 days of the idealized trajectories; filled diamonds are the idealized trajectories for
 325 which SSTs increase and open black diamonds are idealized trajectories with decreasing SSTs. Pink
 326 triangles represent the two example trajectories from Figure 1 in the main text.

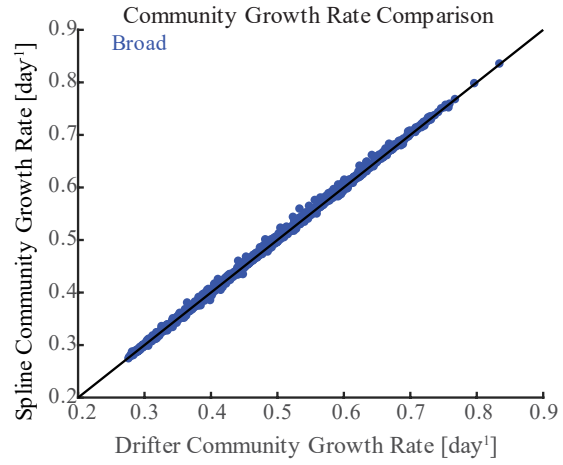
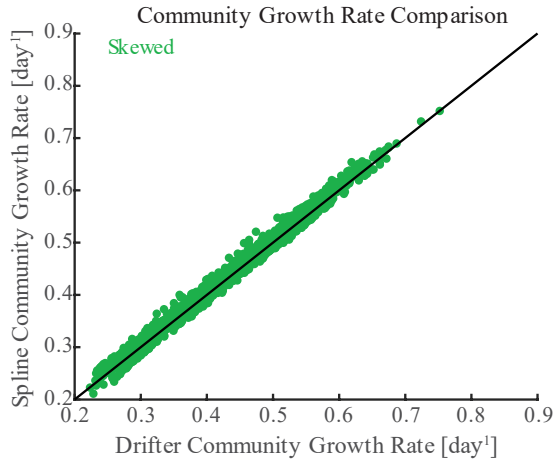
327



328

329 Figure S16. Box plots of the percent of the SST variability in the drifter trajectory that is accounted for by
 330 the smoothed spline. Each of the 2,190 90-day drifter and spline trajectories was broken up into windows
 331 in 1-day increments from 1 to 90 days. The standard deviation of the drifter trajectory is the sum of the
 332 standard deviation of the smoothed spline plus some noise term. From this, the variability accounted for
 333 by the spline for each window, for each trajectory was recorded with the results shown. As expected, over
 334 longer window lengths the spline accounts for higher percentage of the overall variability.

335

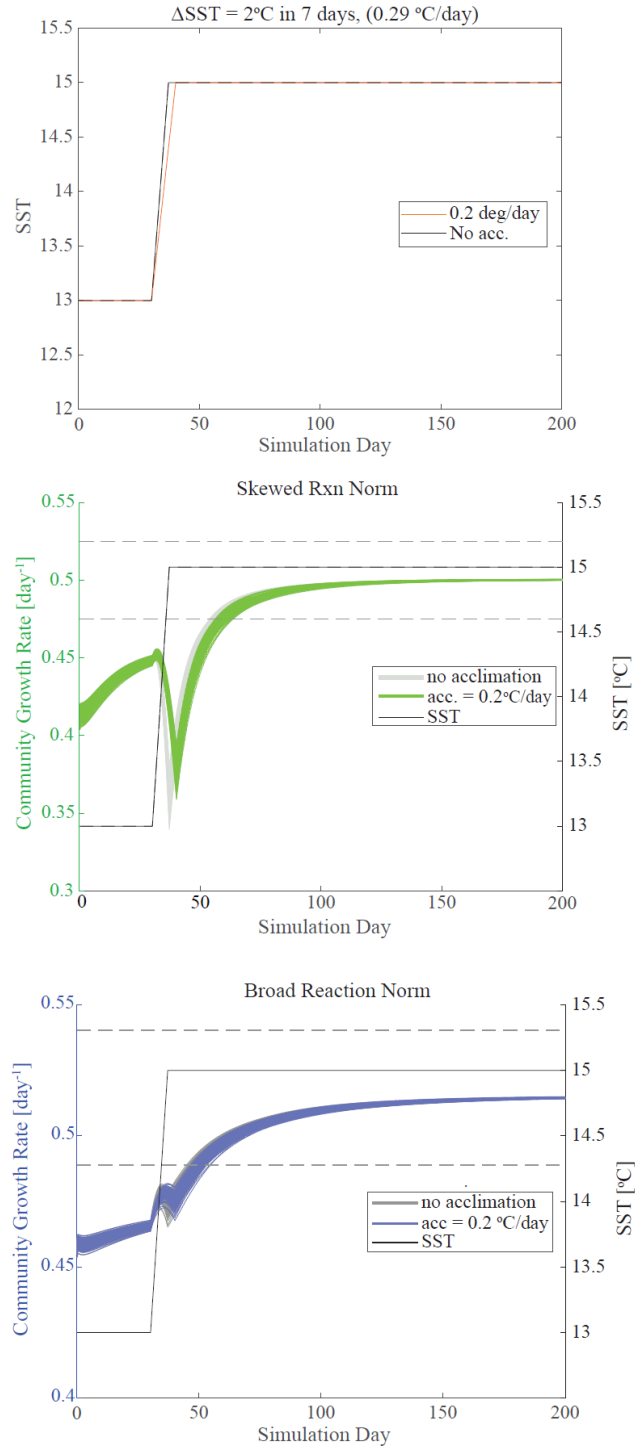


336

337 Figure S17. Comparison of mean community growth rate over the entire 90-day trajectory for the real
 338 trajectories and their spline simulations for skewed (left) and broad (right) shaped reaction norms. With
 339 each reaction norm shape, smoothing the small-scale noise did not impact overall biomass-weighted
 340 community growth rates (95% CI, t-test) further supporting that small-scale noise does not induce a
 341 memory effect.

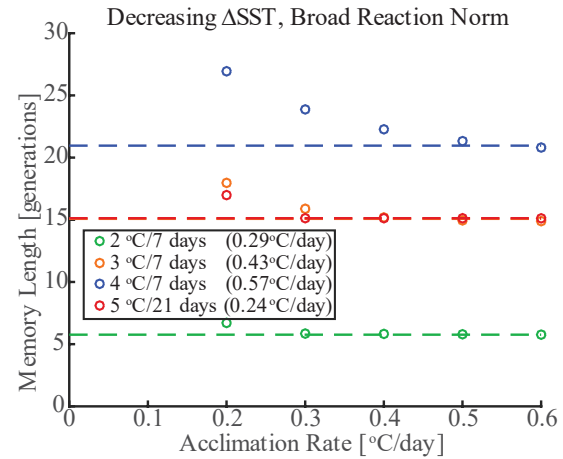
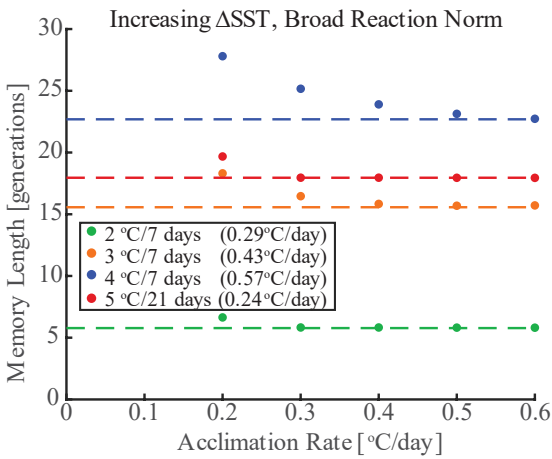
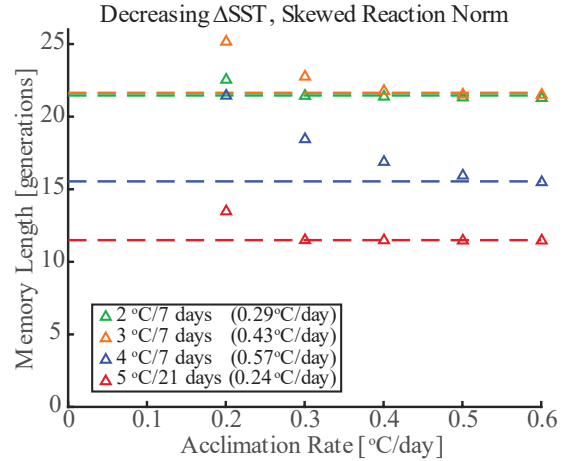
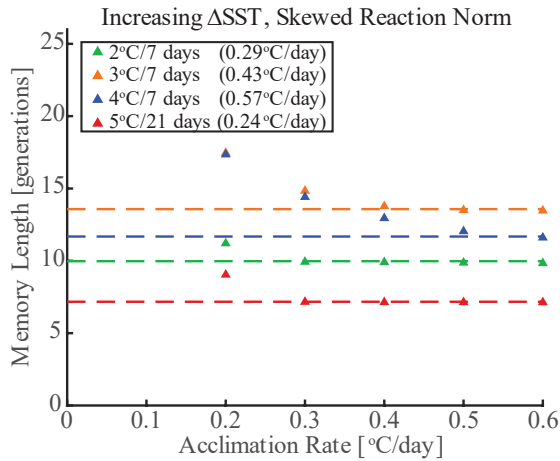
342

343



344

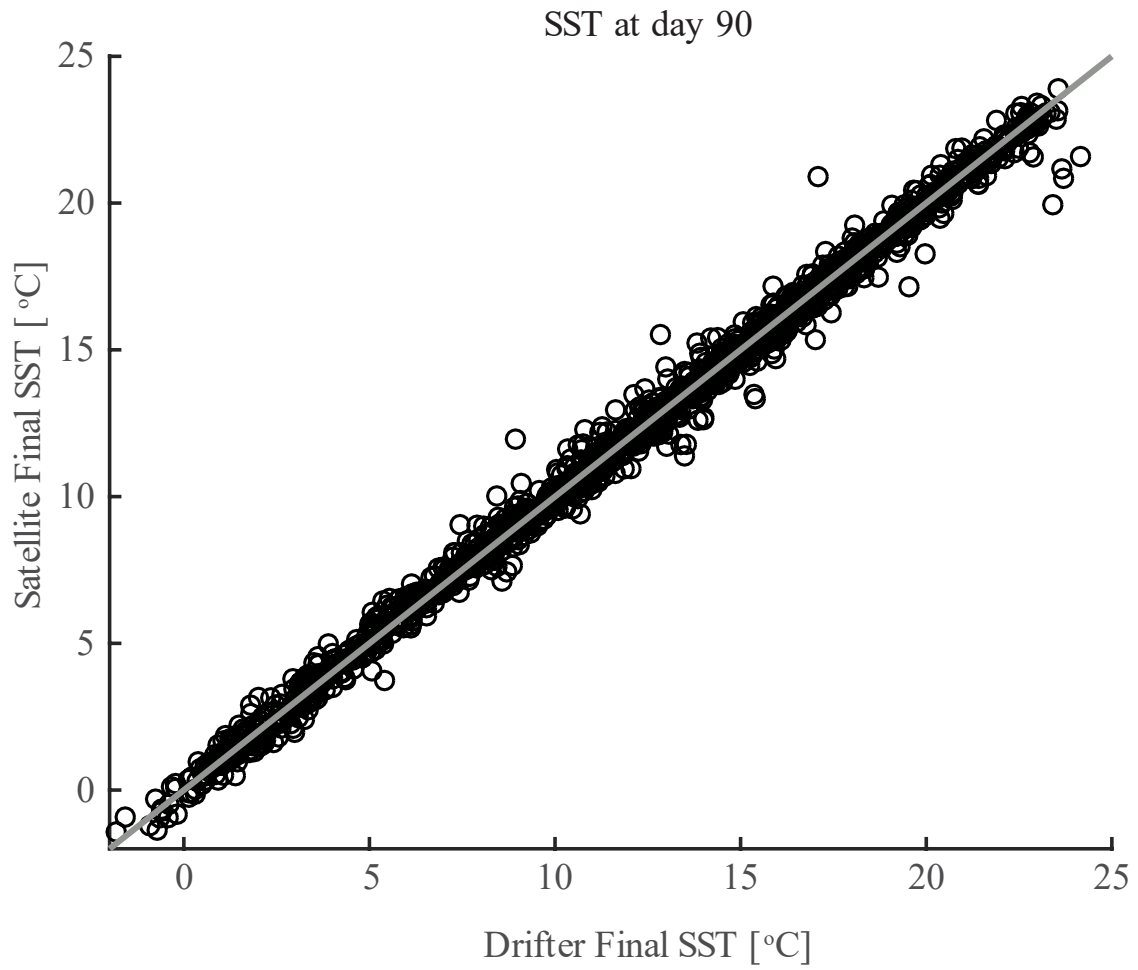
345 Figure S18. Example of impact of acclimation. (Top) Example idealized SST trajectory of changing 2°C
 346 in 7 days with acclimation rates of $0.2^\circ\text{C day}^{-1}$ and $0.3^\circ\text{C day}^{-1}$. Other acclimation rates not shown as they
 347 plot along the No Acclimation line because those rates are faster than the rate of change. (Middle)
 348 Community growth rates for skewed reaction norms over each of the simulations for the no acclimation
 349 simulations (grey lines) and the simulations with an acclimation rate of $0.2^\circ\text{C day}^{-1}$ (green lines). Dashed
 350 lines represent the thresholds used to calculate the memory length. (Bottom) Same as the middle panel
 351 but for broad reaction norms.



352

353 Figure S19. Impact of acclimation on memory length on the skewed reaction norms (top row) and the
 354 broad reaction norms (bottom row) in both the increasing (left column) and decreasing (right column)
 355 Δ SST directions. Dashed lines represent the memory lengths calculated for the simulations that did not
 356 incorporate acclimation. When acclimation rates are greater than or equal to the rate of SST change, there
 357 is no difference between the simulations that incorporated acclimation and those that did not.

358



359

360 Figure S20. Comparison of the final SST for the drifter and the satellite data. The data from both sources
361 represent the same location in space and time so the data should be similar and in fact, are not statistically
362 different from one another (ttest, 95% CI). The grey line represents the 1-1 line.

363

364

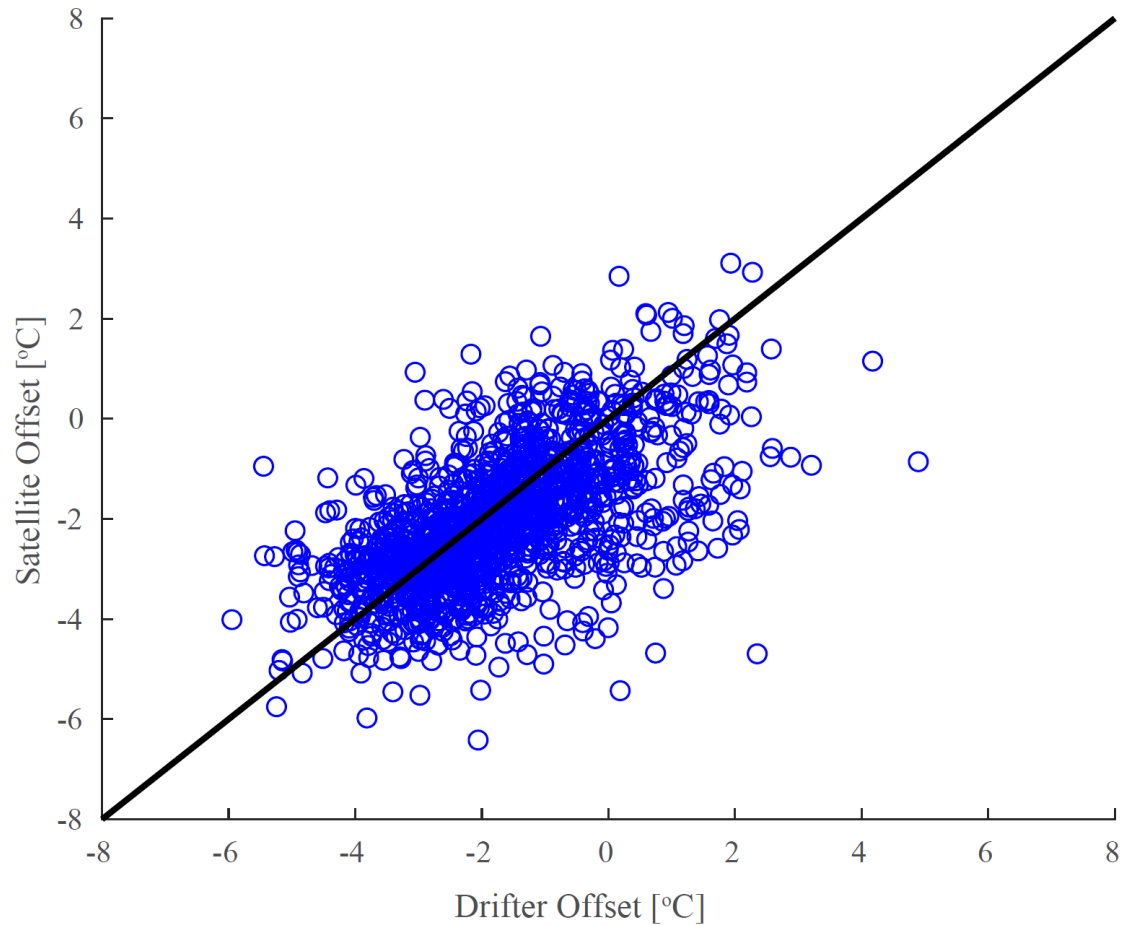
365

366

367

368

369



370

371 Figure S21. Same as Figure 4 in the main text but for broad shaped reaction norms. The impact of
372 Lagrangian and Eulerian variability on community composition. Here we plot the difference between the
373 T_{opt} of the most abundant phenotype at the end of each 90-day trajectory and the final SST for the drifter
374 trajectory (x-axis) and the satellite data (y-axis). The final SSTs for the drifter and satellite data are
375 statistically identical (t-test, 95% CI). Therefore, deviations from the 1:1 line demonstrate the impact of a
376 Lagrangian versus Eulerian reference frame on community composition.

377

378

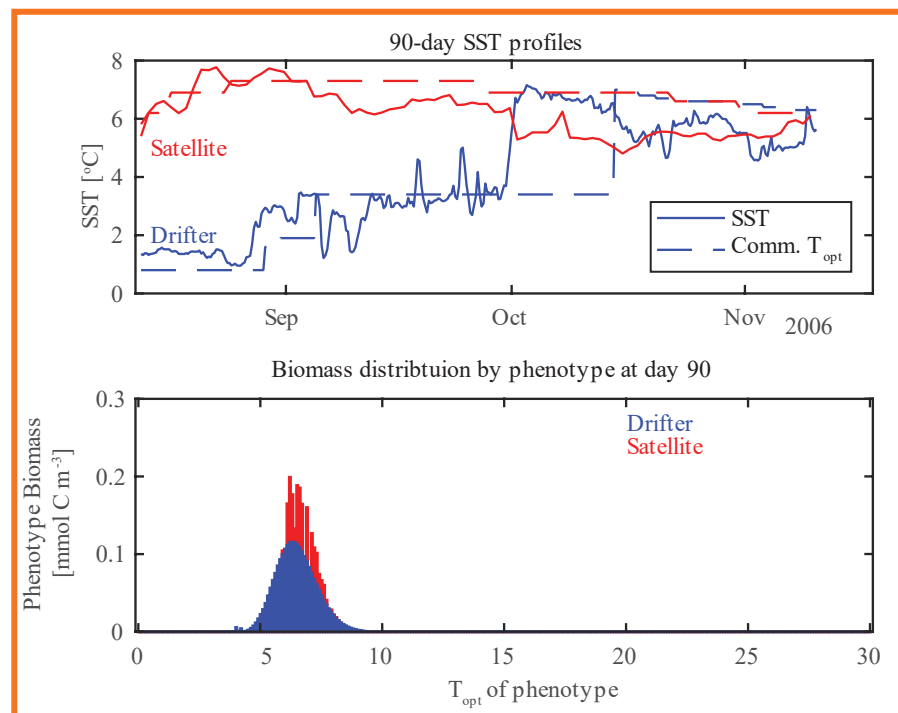
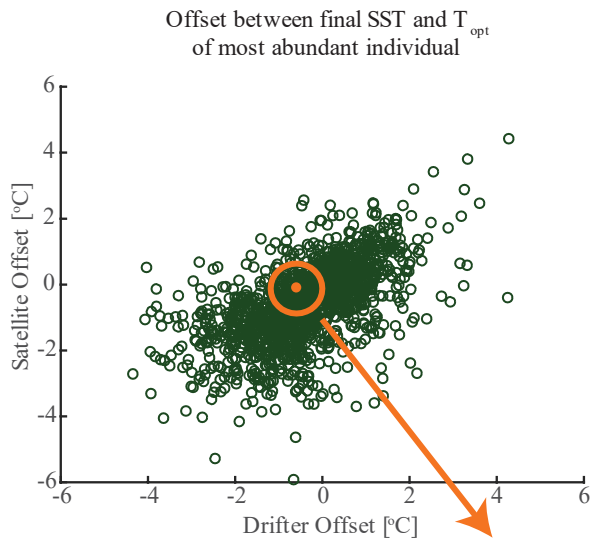
379

380

381

382

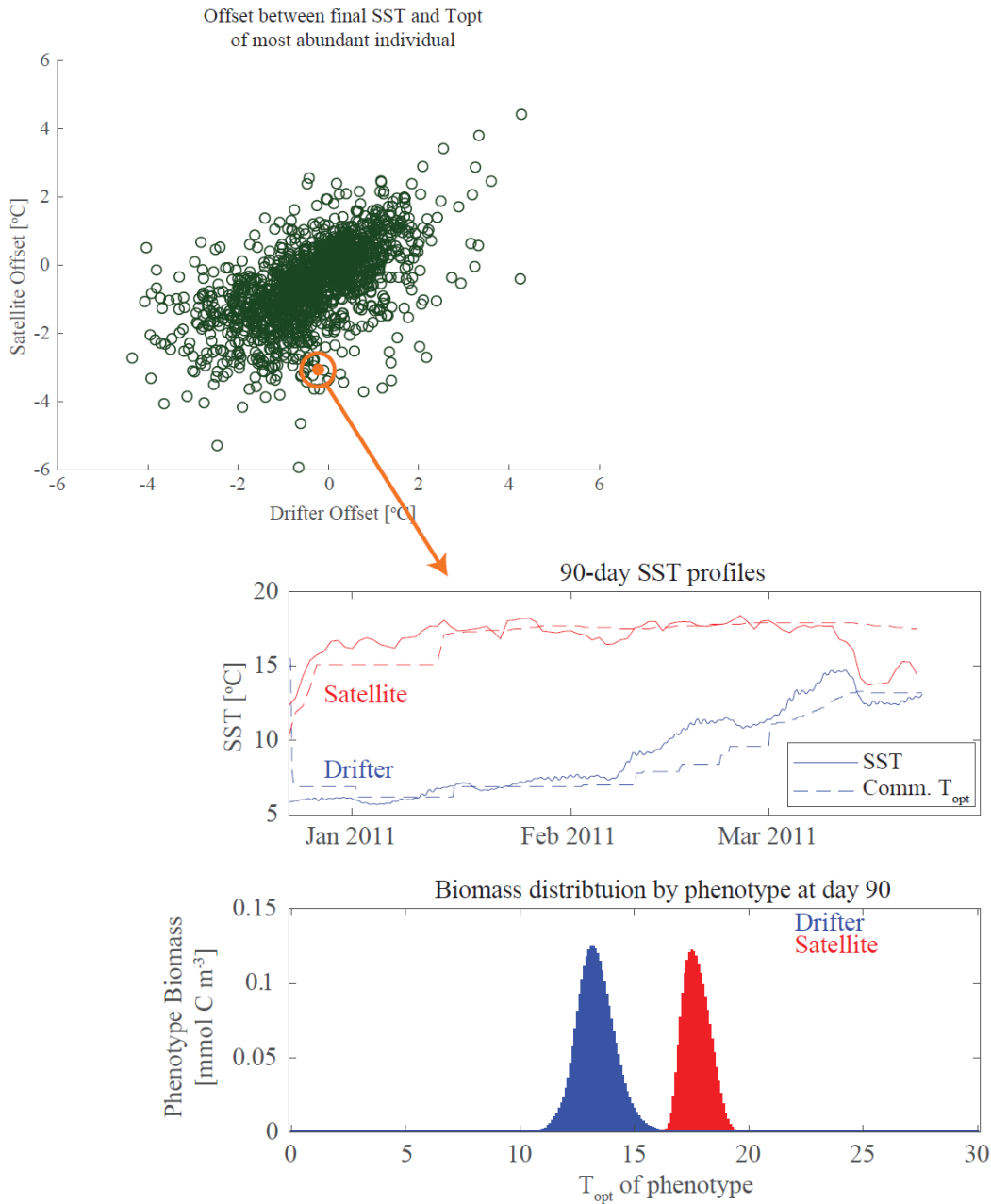
383



384

385 Figure S22. The impact of SST variability on community composition. (Top) An example 90-day drifter trajectory
 386 and the satellite SST data for the final location of the drifter over the same 90 days shown as solid lines. The dashed
 387 lines are the T_{opt} of the most abundant phenotype at each timestep. (Bottom) The biomass of each phenotype with a
 388 skewed shaped reaction norms at day 90 for the satellite and drifter trajectories. In this example, the offset between
 389 the final SST is -0.60°C for the drifter and -0.09°C for the satellite data. The difference in the magnitude of the offset
 390 between the two data sets represents the difference in the variability of the SSTs. However, in this example, the
 391 satellite SSTs stay relatively constant whereas the drifter SSTs experience a rapid increase of 3.5°C in 4 days
 392 beginning Sept. 29. Because the drifter SSTs remain relatively constant through the end of the simulation which results a community T_{opt}
 393 that reflects the SSTs at day 90 for both the satellite and the drifters.

395



396

397 Figure S23. The impact of SST variability on community composition. (Top) An example 90-day drifter
 398 trajectory and the satellite SST data for the final location of the drifter over the same 90 days shown as
 399 solid lines. The dashed lines are the T_{opt} of the most abundant phenotype at each timestep. (Bottom) The
 400 biomass of each phenotype with a skewed shaped reaction norms at day 90 for the satellite and drifter
 401 trajectories. In this example, the offset between the final SST is -0.23°C for the drifter and -3.1°C for the
 402 satellite data. The difference in the magnitude of the offset between the two data sets represents the
 403 difference in the variability of the SSTs. Here, the drifter SSTs gradually increase over the 90 days which
 404 allows the community to continuously track the changes in SST whereas the satellite SSTs are relatively
 405 stable and then rapidly decrease from 17.7°C on March 10 to 13.8°C on March 17. Due to the long
 406 memory effect associated with this rate and magnitude of change, the community was not able to track the
 407 SST change which resulted in a large offset between the final SST and the T_{opt} of the most abundant
 408 phenotype at day 90.